Available online at www.sciencedirect.com
SCIENCE DIRECT®
Chemical Physics Letters 410 (2005) 293–297
CHEMICAL PHYSICS LETTERS
www.elsevier.com/locate/cplett

Signature of electronic correlation in multi-electron emission from C_{60}

O. Kidun, N. Fominykh, J. Berakdar *

Max-Planck Institut für Mikrostrukturphysik, Weinberg 2, 06120 Halle, Germany

Received 16 March 2005; in final form 17 May 2005
Available online 16 June 2005

Abstract

Contrasting single to double-particle transition probabilities induced by a one-particle perturbation yields information on the strength of (two-particle) correlation in a system. Here, we calculate single and double ionization probabilities for a C_{60} molecule upon the absorption of a single photon. We employ the Hartree–Fock and the frozen-core approximations for single-particle states and the random-phase approximation for the screened Coulomb interaction. Energy and angular dependencies of total and differential cross-sections are analyzed and the signature of the geometry of the fullerene and its charge-density response are pointed out.

1. Introduction

The impact of electronic interaction on the physical properties of materials has been the subject of research since the early days of modern physics. The interest in this topic is not only driven by the complexity and the intellectual challenge in describing interacting, many electron systems. In fact, electronic correlation is a key factor for understanding a variety of observable physical phenomena: Wannier excitonic states in wide-band semiconductors, and the insulating (magnetic) ground states of narrow band materials, such as 3d transition metal oxides, rare earths, and actinides are just few examples. The role of electronic correlation in molecular and polymeric materials has been as well in the focus of research. The discovery that C_{60} doped with alkalis may turn superconducting [1] initiated an ongoing investigation of the role of the electron–electron (e–e) interaction in fullerenes: The analysis of the KVV C_{60} Auger results [2] indicated that doped C_{60} has the properties of a strongly correlated system, e.g., it has been argued that K_3C_{60} is a half-filled Mott-Hubbard insulator. A theoretical study of the nature of the e–e interaction in solid (ordered) phase of C_{60} concluded that the screened on-site molecular Coulomb integral U is $U \approx 2.1$ eV [3]. On the other hand, as confirmed by a range of spectroscopic studies (photoemission, inverse photoemission, and soft X-ray absorption [4]), the electronic structure of C_{60} remains essentially intact when a solid is formed. Therefore, it is of interest to study the nature of e–e interaction in isolated C_{60}. In this Letter, we propose to study the e–e interaction of the valence electrons by means of photo-induced single and double electron-removal spectroscopy. The significance of this proposition can be appreciated from the lowest-order (in the e–e interaction) diagram describing the double photoelectron emission (DPE) (cf. Fig. 1): A photon with energy $\hbar\omega$ [5] excites a valence state φ_v to the (vacuum) scattering state $\psi_{\mathbf{q}}$ which is identified by the wave vector $\mathbf{q}$ (the index v stands for a collective set of quantum numbers (including spin) characterizing the orbital φ_v). Measuring the electron emission probability at a specified $\mathbf{q}$ yields information on the

* Corresponding author. Fax: +49 345 5511223.
E-mail addresses: okidun@mpi-halle.de (O. Kidun), jber@mpi-halle.de (J. Berakdar).

0009-2614/$ - see front matter © 2005 Elsevier B.V. All rights reserved.
doi:10.1016/j.cplett.2005.05.088

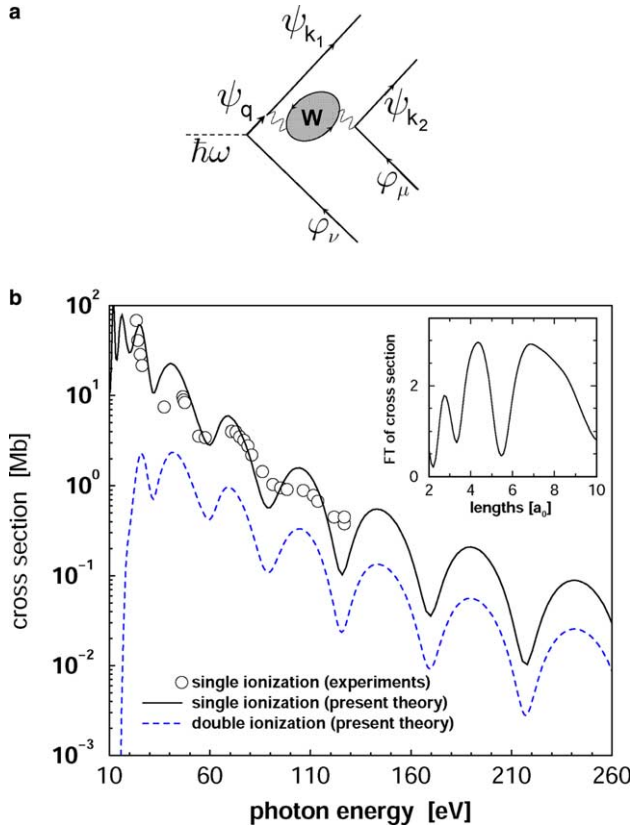

Fig. 1. (a) DPE described by the lowest-order diagram in the electron–electron interaction W. (b) Calculated single σ_1 (solid curve) and double (dashed curve) photoionization cross-sections of the highest occupied molecular orbital (HOMO) of C_{60} vs. photon energy. Open circles are experimental absolute partial σ_1 of HOMO of C_{60} [14]. Inset shows the Fourier transform of $\sigma_1(q)$, where $q = \sqrt{2(\omega + \varepsilon_{\mathrm{HOMO}})}$ is the photoelectron wave vector.

valence single-particle spectrum (which is the aim of single photoelectron spectroscopy SPE [6]). However, there is a finite probability for the excited electron with the wave vector $\mathbf{q}$ to interact with a second valence state φ_μ leading asymptotically to two vacuum electron states $\psi_{\mathbf{k}_1}$ and $\psi_{\mathbf{k}_2}$ with wave vectors $\mathbf{k}_1$ and $\mathbf{k}_2$. These states can be verified in a coincidence experiment. The (VUV) photon couples to a single particle only. Hence, the emission of two photoelectrons can only be mediated by the valence e–e interaction [5]. Obviously, measuring the angular and energy correlation between the two excited electrons yields valuable details that are encompassed in the averaged energetic weight U of the e–e interaction. In C_{60} the electrostatic e–e Coulomb interaction u acts in the presence of an inhomogeneous polarizable surrounding. Thus u will be dynamically (and non-locally) screened. In a linear response approach the screened e–e interaction W is $W = u/\varepsilon$, where $\varepsilon = \varepsilon(\omega, \mathbf{q} - \mathbf{k}_2)$ is the dielectric function. For sufficiently screened u the diagram shown in Fig. 1 is dominant over higher order diagrams that account for further multiple scattering events (in W). Recent theoretical calculations using W within the random phase approximation with exchange (RPAE) [7] indicated a surprisingly strong screening of u in C_{60} [8,9]. This encouraged us to evaluate the SPE and DPE probabilities using the diagram Fig. 1. Besides, the recent experimental activities in realizing DPE from (free and surface-deposited) C_{60} [10,11] make the enormous computational efforts in calculating DPE cross-sections worthwhile and desirable. The application of the present theory for the description of the emission of more than two electrons from C_{60} is currently computationally not possible. Therefore, we introduced in a recent work [13] a statistical photon-energy deposition model for the treatment of the total ionization cross-sections for many-electron emission. A purely statistical treatment (see also related references in [13]) is, however, inappropriate to deal with the simultaneous one-photon two-electron transitions, in particular as far as the two-particle energy and angular correlations are concerned.

2. Theoretical approach

The photon absorption and the electrons emission proceed fast on typical time scales of the ground-state molecule. Hence, degrees of freedom other than those of the valence electrons are frozen during the emission process. The fully differential SPE cross-section $\frac{\mathrm{d}\sigma_1(\omega)}{\mathrm{d}^3\mathbf{q}}$ we evaluate within the dipole approximation as (unless otherwise stated we use atomic units (a.u.) throughout)

$$\frac{\mathrm{d}\sigma_1(\omega)}{\mathrm{d}^3\mathbf{q}} = 4\pi^2\alpha\omega \sum_{\substack{v \\ \varepsilon_v \leqslant E_\mathrm{F}}} \left|\langle\psi_\mathbf{q}|\mathbf{e}\cdot\mathbf{r}|\varphi_v\rangle\right|^2 \delta(\omega + \varepsilon_v - E_q). \quad (1)$$

where $\mathbf{e}$ is the (linear) polarization vector of the light, ε_v is the energy of the occupied state φ_v. E_F is the highest occupied molecular state (HOMO), E_q is the photoelectron energy and α is the fine-structure constant. The total SPE cross-section is obtained by integrating numerically over $\mathbf{q}$. The SPE has been already calculated by a number of authors (e.g., [24,23,13] and references therein). An example of the partial σ_1, from HOMO is shown in Fig. 1 (determining ω and E_q pins down ε_v in Eq. (1)). The fully differential double ionization cross-section $\frac{\mathrm{d}\sigma_2(\omega)}{\mathrm{d}^3\mathbf{k}_1\mathrm{d}^3\mathbf{k}_2}$ is evaluated as

$$\frac{\mathrm{d}\sigma_2(\omega)}{\mathrm{d}^3\mathbf{k}_1\mathrm{d}^3\mathbf{k}_2} = \sum_{\mu,\varepsilon_\mu \leqslant E_\mathrm{F}} \int \mathrm{d}^3\mathbf{q} \left|\langle\Psi_{\mathbf{k}_1\mathbf{k}_2}|W|\varphi_\mu\psi_\mathbf{q}\rangle\right|^2 \frac{\mathrm{d}\sigma_1(\omega)}{\mathrm{d}^3\mathbf{q}} \times \delta(E_\mathbf{q} + \varepsilon_\mu - E_1 - E_2), \quad (2)$$

where $\Psi_{\mathbf{k}_1\mathbf{k}_2}$ is an anti-symmetrized two-electron scattering wave function constructed from the one-electron

states $\psi_{\mathbf{k}_1}$ and $\psi_{\mathbf{k}_2}$. Thus, $\langle \Psi_{\mathbf{k}_1\mathbf{k}_2}|W|\varphi_\mu\psi_{\mathbf{q}}\rangle$ contains a direct and an exchange term which we will treat as in our previous work [8] on electron-impact ionization. The direct amplitude $\langle\psi_{\mathbf{k}_1}\psi_{\mathbf{k}_2}|W|\varphi_\mu\psi_{\mathbf{q}}\rangle$ is determined by solving full numerically the integral RPAE equation (similarly we calculate the exchange term)

$$\begin{aligned}\langle\psi_{\mathbf{k}_1}\psi_{\mathbf{k}_2}|W|\varphi_\mu\psi_{\mathbf{q}}\rangle &= \langle\psi_{\mathbf{k}_1}\psi_{\mathbf{k}_2}|u|\varphi_\mu\psi_{\mathbf{q}}\rangle \\ &+ \sum_{\substack{p,\varepsilon_p\leqslant E_F\\ h,\varepsilon_h>E_F}}\left(\frac{\langle\varphi_p\psi_{\mathbf{k}_2}|W|\varphi_\mu\varphi_h\rangle\langle\varphi_h\psi_{\mathbf{k}_1}|u|\psi_{\mathbf{q}}\varphi_p\rangle}{E_{\mathbf{q}}-(\varepsilon_p-\varepsilon_h-\mathrm{i}\delta)}\right. \\ &\left.-\frac{\langle\varphi_h\psi_{\mathbf{k}_2}|W|\varphi_\mu\varphi_p\rangle\langle\varphi_p\psi_{\mathbf{k}_1}|u|\psi_{\mathbf{q}}\varphi_h\rangle}{E_{\mathbf{q}}+(\varepsilon_p-\varepsilon_h-\mathrm{i}\delta)}\right),\end{aligned} \tag{3}$$

where φ_p and φ_h are, respectively, the intermediate particle and hole states and δ is a small positive real number. Neglecting the influence of the charge-density fluctuations amounts to using the first term on the RHS of Eq. (3) only (referred to below as w/o RPAE). Neglecting altogether the correlation *between* the two photoelectrons, i.e., setting $W \equiv constant$, the double ionization cross-section vanishes (in our calculations scattering and bound states belong to the same Hamiltonians and hence they do not overlap). The various integral cross-sections are obtained from Eq. (2) by a numerical integration (using a Monte Carlo procedure) over the appropriate variables $(E_1,\ E_2,\ \hat{\mathbf{k}}_1,\ \hat{\mathbf{k}}_2)$.

3. Numerical procedure

The single-particle states of the fullerene are obtained from self-consistent Hartree–Fock calculations using an implementation of the non-local variable phase method [15,16]. Hence, we incorporate in the *initial state* (ground state) the mean-field part of the electron–electron interactions and exchange effects. As done in various studies on the electronic properties of C_{60} we employ a spherical shell model potential $V_{\mathrm{ion}}(r)$ for the 240 valence electrons ([17,8] and references therein), i.e., $V_{\mathrm{ion}}(r) = V_0$ for $R-\delta < r < R$, and $V_{\mathrm{ion}}(r) = 0$ elsewhere. In determining the model potential V_{ion} one needs the experimental radius of C_{60} ($R \approx 6.65$ a.u.), the (average) distance between the neighboring carbon sites (which enters as the thickness of the well $\delta \approx 2.69$ a.u.) and the affinity energy of the electron to the singly charged fullerene [18]. The number of the valence electrons (240) and the experimentally determined first ionization potential of C_{60} (7.6 eV [20,21]) fix then the potential depth $V_0 \approx 108$ eV. Here we do not discuss the resulting ground-state electronic structure for space limitation and refer to [19] which uses a similar model and where the ground-state spectral properties of C_{60} are compared to experiments. Our procedure produces results numerically similar to [19].

4. Results and interpretations

A notable feature of the photoionization cross-sections σ_1 and σ_2 shown in Fig. 1 is the oscillations as a function of ω. As discussed in [14,22–24], the origin of the oscillations in σ_1 lies in an interference effect of the photoelectron waves emitted from parts of the potential that scatter particularly strong. In practice, these sites are the potential discontinuities at the carbon nuclei positions which enter in our model as the width δ of the confining ionic potential, whereas the C_{60} icosahedrical symmetry is approximated by a spherical one. Therefore, the two characteristic lengths R and δ of our model are manifested in σ_1 as two resonant frequencies and two satellites corresponding to δ, $R-\delta$, R and $R+\delta$, as shown in the inset of Fig. 1. It should be stressed, however, that this simple explanation is not generally viable even in the present model calculations [25] because in addition to the confining potential, the electrons are also subject to the (non-local) Hartree–Fock and the centrifugal potential. The results in Fig. 1 indicate, however, that in this particular case the confining potential plays the key role, as far as the oscillations in σ_1 are concerned. The oscillation appears in σ_2 for the following reason: Inspecting the diagram Fig. 1 we conclude that only in the photon absorption step the energy $\hbar\omega$ must be converted into momentum $\mathbf{q}$ by a strong scatterer in the absorption region. In contrast, the e–e scattering potential W can in general mediate momentum and energy exchange and therefore the cross-section for this process is not expected to show any oscillations (when varying ω). This is in fact confirmed theoretically [8] and experimentally [26,27] by the electron-impact ionization of C_{60}. In addition, the particle–hole (de)excitations, as incorporated in Eq. (3) have been shown to flatten the e–e scattering probability [8]. That is, as far as $\sigma_2(\omega)$ vs. ω is concerned, in Eq. (2) the term $\int \mathrm{d}^3\mathbf{k}_1\mathrm{d}^3\mathbf{k}_2\left|\langle\Psi_{\mathbf{k}_1\mathbf{k}_2}|W|\varphi_\mu\psi_{\mathbf{q}}\rangle\right|^2$ acts as a smooth flat function of ω and hence $\sigma_2(\omega)$ exhibits the oscillations present in σ_1 as well as qualitatively the same slope. The ratio of $\sigma_1(\omega)$ to $\sigma_2(\omega)$ at a particular ω is a general indicator of the strength of W ($\lim_{W\to 0}\sigma_2 \to 0$ as clear from Fig. 1). At present, we cannot compare directly with the (initial-state non-resolved) experiments [10–12] due to computational limitations. Experimentally, Reinköster et al. [11] reported a ratio of 1/7 between angle- and energy-integrated double and single ionization events at a photon energy of 45 eV, whereas Kou et al. [10] find a ratio of about 2/3. A different ratio is found in the condensed phase [12], however, the cross-sections are then measured for a certain electron emission angles.

Detailed information on the energy- and angular correlation are accessed by studying the differential cross-sections. For example, Fig. 2 shows, for fixed total energies of the pair $E_{\mathrm{tot}} = E_1 + E_2$, the sharing of E_{tot}

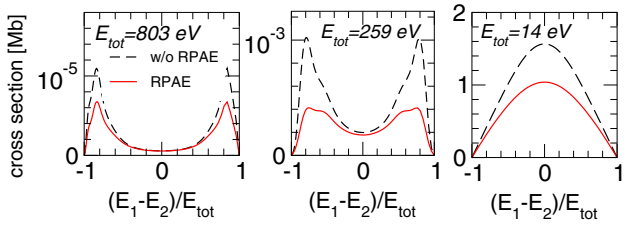

Fig. 2. Angular-integrated sharing distributions of the fixed energy $E_{\rm tot} = E_1 + E_2$ between two electrons emitted upon one-photon double ionization of C_{60} HOMO.

between the two electrons. A strong suppression of $\frac{d\sigma_2(\omega)}{dE_1 dE_2}$ is observed due charge-density fluctuations, which is consistent with previous conclusions that the screening caused by these fluctuations reduces considerably the effective scattering region and hence the scattering cross-section [8,26,27]. On the other hand the shape of $\frac{d\sigma_2(\omega)}{dE_1 dE_2}$ differs qualitatively from its atomic counterpart [28–30]. In the latter case the cross-section does not show at low energies an abrupt decrease when $E_{1,2} \to 0$. This can be traced back to kinematical and dynamical reasons: From Eq. (2), we conclude that $\frac{d\sigma_2(\omega)}{dE_1 dE_2 d^2\hat{\mathbf{k}}_1 d^2\hat{\mathbf{k}}_2} = k_1 k_2 \frac{d\sigma_2(\omega)}{d^3\mathbf{k}_1 d^3\mathbf{k}_2}$. Hence, for kinematical reasons $\frac{d\sigma_2(\omega)}{dE_1 dE_2}$ should decrease as $\sqrt{E_{1,2}}$ for $E_{1,2} \to 0$. On the other hand, the (Coulomb) density of states, DOS, for an attractive $-1/r_{1,2}$ potential diverges as $1/k_{1,2}$ for $k_{1,2} \to 0$ (leading in this limit to phenomena known as the target cusp or the electron capture to the continuum cusp in the electron-emission spectra, cf. [31] and references therein). For atomic processes the $1/k_{1,2}$ divergence of DOS for $k_{1,2} \to 0$ removes the kinematical $k_{1,2} \to 0$ decrease. In contrast, as outlined above, the C_{60} single particle potentials do not have $-1/r_{1,2}$ behaviour and DOS(C_{60}) is finite at $k_{1,2} \to 0$. Thus, due to kinematics $\frac{d\sigma_2(\omega)}{dE_1 dE_2}$ vanishes for $E_{1,2} \to 0$, as seen in Fig. 2. The shape of the energy-sharing correlation curve has its origin in the double Fourier transform (FT) $\tilde{W}$ (form factor) of W: for large momentum transfers (implying $\omega \gg E_F$) $\tilde{W}$ behaves as $\tilde{W} \propto 1/|\mathbf{q} - \mathbf{k}_1|^2$ ($\mathbf{q}, \mathbf{k}_1$ are shown in Fig. 1). Thus, e–e scattering events are predominant in which one fast electron and one slow electron are produced. On the other hand, $\lim_{E_{1,2}\to 0} \frac{d\sigma_2(\omega)}{dE_1 dE_2} \to 0$ holds resulting in the shapes of $\frac{d\sigma_2(\omega)}{dE_1 dE_2}$, observed in Fig. 2 for $\omega \gg E_F$. At low photon energies the momentum transfer is necessarily small. Due to screening we find that $\tilde{W}$ (at fixed small ω) is basically independent of E_1 and E_2[1] which (in combination with $\lim_{E_{1,2}\to 0}\sigma_2(E_1, E_2) \to 0$) makes comprehensible the low-frequency behaviour of the shape of $\frac{d\sigma_2}{dE_1 dE_2}$, as revealed by Fig. 2.

[1] $W(r) \propto e^{-r/\lambda}/r$ holds for a homogenous system in the long wavelength limit. $\lambda \in \mathbb{R}^+$ is a screening length. FT of W, $\tilde{W}(k) \propto 1/(k^2 + \frac{1}{\lambda^2})$ is constant for $k \ll \frac{1}{\lambda}$.

As to be expected the RPA corrections are frequency dependent and diminish for $\omega \gg E_F$ in which case the e–e scattering takes place in a much shorter time compared to the characteristic response time of the charge density (in this case $\lim_{\omega\gg E_F} W \to u$). In Fig. 3 the dependence of $\frac{d\sigma_2(\omega)}{dE_1 dE_2}$ on E_2 is plotted for a fixed E_1 in which case the oscillation akin to photoionisation from C_{60} emerge. We note the frequency-dependent influence of screening on the oscillations.

Another correlation feature accessible by DPE is the angular correlation of the two electrons, as quantified by $\frac{d\sigma_2}{dE_1 dE_2 d^2\hat{\mathbf{k}}_1 d^2\hat{\mathbf{k}}_2}$ for fixed E_1 and E_2. The general behaviour of this quantity is currently in the focus of discussion in atomic and molecular physics [28–30], in particular for simple targets such as noble gas atoms. For C_{60}, even though the assumed spherical symmetry of the problem brings about some simplifications an understanding of all the facets of $\frac{d\sigma_2}{dE_1 dE_2 d^2\hat{\mathbf{k}}_1 d^2\hat{\mathbf{k}}_2}$ is a challenge. The example in Fig. 4 demonstrates the strong dependence of $\frac{d\sigma_2}{dE_1 dE_2 d^2\hat{\mathbf{k}}_1 d^2\hat{\mathbf{k}}_2}$ on the charge-density fluctuations (which are negligible for targets with large level spacing). The

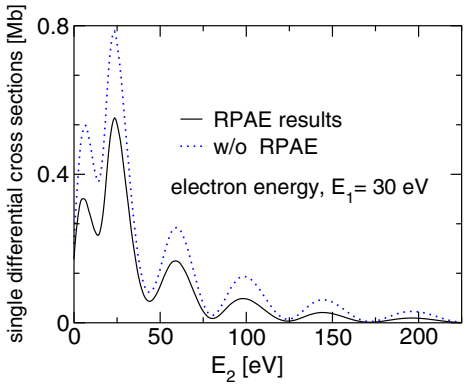

Fig. 3. Same cross-sections as in Fig. 2, however, one electron has a fixed energy (E_1 = 30 eV); the energy E_2 of the second is scanned by varying the photon energy. Results with (without) RPAE corrections are shown by the solid (dotted) curve.

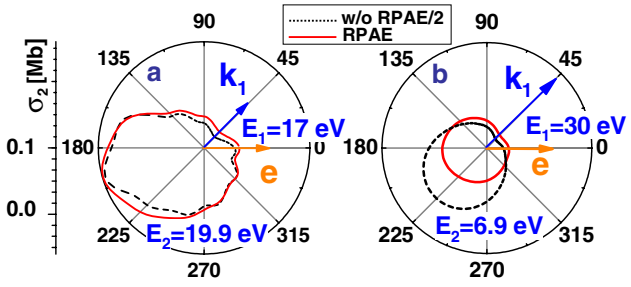

Fig. 4. The angular correlation between two electrons emitted from HOMO with fixed energies $E_{1,2}$ (shown on the figures) at $\hbar\omega$ = 50 eV. σ_2 is measured in Mbarn. The electron having E_1 is fixed under 45° with respect to the photon polarization vector **e**. The results without RPA are scaled down by factor 2.

reason for these variations with $\hat{\mathbf{k}}_1, \hat{\mathbf{k}}_2$ is the dependence of the dielectric response (described by Eq. (3)) on the momentum transfer during the e–e scattering. Therefore, a measurement of the angular correlation as depicted in Fig. 4 reveals, for a fixed frequency, the anisotropic (momentum-transfer dependent) screening of W in addition to the angular correlation between the electrons. Fig. 4a reveals a smearing of the e–e repulsion for $\hat{\mathbf{k}}_1 \| \hat{\mathbf{k}}_2$ due to charge-density fluctuations and integrations over $\mathbf{q}$ in Eq. (3). In addition, $\frac{d\sigma_1}{d^3\mathbf{q}}$ has a rich structure which (due to Eq. (2)) is reflected in the peaks observed in Fig. 4a.

5. Conclusions

Summarizing, we present a theory that describes, at the same footing, photo-induced single and double valence-electron removals from clean, isolated C_{60}. We demonstrated the power of DPE in revealing the details of the (non-local) frequency-dependent electron–electron interaction in C_{60}. In view of the results of [1] on the superconducting properties of alkalis-doped C_{60} it is valuable to extend SPE and DPE studies to doped C_{60}.

References

[1] A.F. Hebard, M.J. Rosseinsky, R.C. Haddon, D.W. Murphy, S.H. Glarum, T.T.M. Palstra, A.P. Ramirez, A.R. Kortan, Nature 350 (1991) 600.
[2] R.W. Lof, M.A. vanVeenendaal, B. Koopmans, H.T. Jonkman, G.A. Sawatzky, Phys. Rev. Lett. 68 (1992) 3924.
[3] D.P. Joubert, J. Phys.: Condens. Matter 5 (1993) 8047.
[4] K.-D. Tsuei, J.Y. Yuh, C.-T. Tzeng, R.-Y. Chu, S.-C. Chung, K.-L. Tsang, Phys. Rev. B 56 (1997) 15412.
[5] We limit the discussion to photon energies below the threshold for KVV C_{60} Auger transitions.
[6] S. Hüfner, in: Photoelectron Spectroscopy, Springer Series in Solid-State Science, vol. 82, Spinger, Berlin, 1995.
[7] A.L. Fetter, J.D. Walecka, Quantum Theory of Many-particle Systems, McGraw-Hill, New York, 1971.
[8] O. Kidun, J. Berakdar, Phys. Rev. Lett. 87 (2001) 263401.
[9] O. Gunnarsson, G. Zwicknagel, Phys. Rev. Lett. 69 (1992) 957.
[10] J. Kou, T. Mori, S.V.K. Kumar, Y. Hariyama, Y. Kubozono, K. Misuke, J. Chem. Phys. 120 (2004) 6005.
[11] A. Reinköster, S. Korica, G. Prumper, J. Viefhaus, K. Godehusen, O. Schwarzkopf, M. Mast, U. Becker, J. Phys. B 37 (2004) 2135.
[12] F.U. Hillebrecht, A. Morozov, J. Kirschner, Phys. Rev. B 71 (2005) 125406/1-6.
[13] O. Kidun, N. Fominykh, J. Berakdar, J. Phys. B 37 (2004) L321.
[14] U. Becker, O. Gessner, A. Rüdel, J. Electron. Spectrosc. Relat. Phenom. 108 (2000) 189.
[15] O. Kidun, N. Fominykh, J. Berakdar, J. Phys. A. 35 (2002) 9413.
[16] F. Calogero, Variable Phase Approach to Potential Scattering, Academic Press, New York, 1967.
[17] M. Brack, Rev. Mod. Phys. 65 (1993) 677.
[18] E. Tossati, N. Manini, Chem. Phys. Lett. 223 (1994) 61.
[19] S. Keller, E. Engel, Chem. Phys. Lett. 299 (1999) 165.
[20] P. Scheier, B. Dunser, R. Worgotter, M. Lezius, R. Robl, T.D. Märk, Int. J. Mass Spectrom. Ion Process. 138 (1994) 77.
[21] H. Steger, J. Holzapfel, A. Hielscher, W. Kamke, I.V. Hertel, Chem. Phys. Lett. 234 (1995) 455.
[22] A. Rüdel, R. Hentges, U. Becker, H.S. Chakraborty, M.E. Madjet, J.M. Rost, Phys. Rev. Lett. 89 (2002) 125503.
[23] O. Frank, J.M. Rost, Chem. Phys. Lett. 271 (1997) 367.
[24] S.J. Hasegawa, T. Miyamae, K. Yakushi, K. Inokuchi, K. Seki, N. Ueno, Phys. Rev. B 58 (1998) 4927.
[25] O. Kidun, N. Fominykh, J. Berakdar, unpublished.
[26] S. Matt, B. Dünser, M. Lezius, K. Becker, A. Stamatovic, P. Scheier, T.D. Märk, J. Chem. Phys. 105 (1996) 1880.
[27] V. Foltin, M. Foltin, S. Matt, P. Scheier, K. Becker, H. Deutsch, T.D. Märk, Chem. Phys. Lett. 289 (1998) 181.
[28] J. Briggs, V. Schmidt, J. Phys. B 33 (2000) R1.
[29] G.C. King, L. Avaldi, J. Phys. B 33 (2000) R215.
[30] L. Malegat, P. Selles, A. Huetz, J. Phys. B 30 (1997) 251.
[31] J. Ullrich, V. Shevelko (Eds.), Many-particle Quantum Dynamics in Atomic and Molecular Fragmentation, Springer, Berlin, 2003.